LANGMUIR

Adsorption of Small Cationic Nanoparticles onto Large Anionic Particles from Aqueous Solution: A Model System for Understanding Pigment Dispersion and the Problem of Effective Particle Density

S. M. North,[†] E. R. Jones,[*,†] G. N. Smith,[†] O. O. Mykhaylyk,[†] T. Annable,[‡] and S. P. Armes[*,†]

[†]Department of Chemistry, University of Sheffield, Dainton Building, Brook Hill, Sheffield, South Yorkshire S3 7HF, U.K.
[‡]Lubrizol Limited, Hexagon Tower, P.O. Box 42, Blackley, Manchester M9 8ZS, U.K.

S *Supporting Information*

ABSTRACT: The present study focuses on the use of copolymer nanoparticles as a dispersant for a model pigment (silica). Reversible addition−fragmentation chain transfer (RAFT) alcoholic dispersion polymerization was used to synthesize sterically stabilized diblock copolymer nanoparticles. The steric stabilizer block was poly(2-(dimethylamino)ethyl methacrylate) (PDMA) and the core-forming block was poly(benzyl methacrylate) (PBzMA). The mean degrees of polymerization for the PDMA and PBzMA blocks were 71 and 100, respectively. Transmission electron microscopy (TEM) studies confirmed a near-monodisperse spherical morphology, while dynamic light scattering (DLS) studies indicated an intensity-average diameter of 30 nm. Small-angle X-ray scattering (SAXS) reported a volume-average diameter of 29 ± 0.5 nm and a mean aggregation number of 154. Aqueous electrophoresis measurements confirmed that these $PDMA_{71}-PBzMA_{100}$ nanoparticles acquired cationic character when transferred from ethanol to water as a result of protonation of the weakly basic PDMA chains. Electrostatic adsorption of these nanoparticles from aqueous solution onto 470 nm silica particles led to either flocculation at submonolayer coverage or steric stabilization at or above monolayer coverage, as judged by DLS. This technique indicated that saturation coverage was achieved on addition of approximately 465 copolymer nanoparticles per silica particle, which corresponds to a fractional surface coverage of around 0.42. These adsorption data were corroborated using thermogravimetry, UV spectroscopy and X-ray photoelectron spectroscopy. TEM studies indicated that the cationic nanoparticles remained intact on the silica surface after electrostatic adsorption, while aqueous electrophoresis confirmed that surface charge reversal occurred below pH 7. The relatively thick layer of adsorbed nanoparticles led to a significant reduction in the effective particle density of the silica particles from 1.99 g cm^{-3} to approximately 1.74 g cm^{-3}, as judged by disk centrifuge photosedimentometry (DCP). Combining the DCP and SAXS data suggests that essentially no deformation of the PBzMA cores occurs during nanoparticle adsorption onto the silica particles.

Effective particle density for a nanoparticle-stabilized pigment
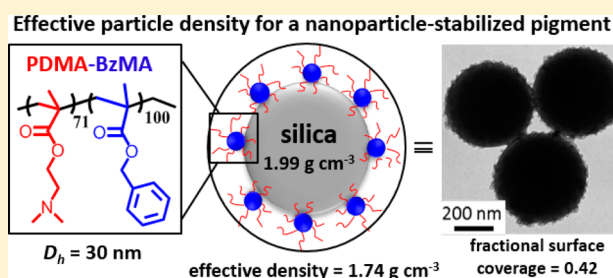
INTRODUCTION

It has been known for more than five decades that amphiphilic AB diblock copolymers can undergo spontaneous self-assembly in solution.[1−4] Various copolymer morphologies can be obtained depending on the diblock composition, including spherical micelles, worm-like particles, or vesicles.[5−20] It is also well-known that a range of diblock copolymers can be used as dispersants for numerous inorganic and organic pigments.[21−27] For example, diblock copolymer micelles have been adsorbed onto polystyrene (PS) latex, silica, or carbon black.[28−30] Similarly, we reported that a commercial hydrogenated polyisoprene−polystyrene diblock copolymer can form star-like spherical micelles in *n*-dodecane and hence act as a dispersant for carbon black[31] or diesel soot.[32]

Many research groups have reported that polymerization-induced self-assembly (PISA) offers an efficient and versatile route to a wide range of well-defined diblock copolymer nanoparticles.[33−35] One important advantage of this approach is that the copolymer is prepared directly in the form of nanoparticles at high solids, which eliminates any requirement for post-polymerization processing. Depending on the choice of monomers, colloidally stable nanoparticle dispersions can be obtained in water, ethanol, or *n*-alkanes.[20,35−39] Of particular relevance to the present work, poly(2-(dimethylamino)ethyl methacrylate)−poly(benzyl methacrylate) (PDMA−PBzMA) copolymer nanoparticles can be prepared directly in either ethanol or ethanol/water mixtures using reversible addition−fragmentation chain transfer (RAFT) dispersion polymerization.[40−43]

There is a considerable volume of literature describing the controlled adsorption of small particles onto larger particles.[30,44,45] Depending on the conditions used, this is

sometimes known as heteroflocculation or heterocoagulation.[46−49] Well-known examples include the electrostatic adsorption of a submicrometer-sized anionic PS latex onto a micrometer-sized cationic PS latex,[50] the heterocoagulation of a small cationic poly(butyl methacrylate) latex onto a large anionic PS latex followed by thermal annealing,[51] and the adsorption of globular proteins onto polypyrrole particles.[52]

Previously, we reported the adsorption of 20 nm-diameter silica nanoparticles onto 463 or 616 nm diameter poly(2-vinylpyridine) latexes.[53] Such heteroflocculation offers an interesting and potentially rather generic route to colloidal nanocomposite particles.[54,55] In the present study, we examine a complementary system comprising small cationic diblock copolymer nanoparticles adsorbed onto large anionic silica particles. The former component can now be readily accessed using PISA formulations[40−43] while the latter colloidal substrate is commercially available with narrow particle size distributions over a range of mean diameters. In principle, such nanoparticle-coated silica particles are a useful model system for understanding the behavior of certain paint and coating formulations. For example, copolymer nanoparticles are sometimes adsorbed onto titania particles to maximize their gloss potential.[56] They may also offer new opportunities for the preparation of colloidally stable inkjet inks[57] or carbon nanotube dispersions.[58]

■ EXPERIMENTAL SECTION

Synthesis of PDMA$_{71}$ Macromolecular Chain Transfer Agent (Macro-CTA) via RAFT Solution Polymerization. A round-bottomed flask was charged with 2-(dimethylamino)ethyl methacrylate (DMA; 60.0 g), 4-cyano-4-(2-phenylethanesulfanylthiocarbonyl)-sulfanylpentanoic acid (PETTC; 1.30 g; synthesized as reported by Jones et al.[41]), 4,4-azobis(4-cyanovaleric acid) (ACVA) initiator (1.1 mg), and tetrahydrofuran (THF; 60 g). This formulation corresponds to a target degree of polymerization (DP) of 75 (assuming perfect RAFT agent efficiency) and a macro-CTA/ACVA molar ratio of 10. The sealed reaction vessel was purged with nitrogen and placed in a preheated oil bath at 66 °C for 8.5 h. The crude PDMA homopolymer (DMA conversion = 75%; M_n = 11 500 g mol^{-1}, and M_w/M_n = 1.24) was purified by precipitate into excess petroleum ether. The mean DP of this PDMA macro-CTA was calculated to be 71, using proton nuclear magnetic resonance (^{1}H NMR) spectroscopy by comparing integrated signals corresponding to the aromatic protons at 7.2−7.4 ppm with those assigned to the methacrylic backbone at 0.4−2.5 ppm.

Synthesis of PDMA$_{71}$−PBzMA$_{100}$ Diblock Copolymer Nanoparticles via RAFT Dispersion Polymerization. A typical protocol for the synthesis of PDMA$_{71}$−PBzMA$_{100}$ diblock copolymer nanoparticles at 15% w/w solids is as follows: benzyl methacrylate (BzMA, 5.0 g), PDMA$_{71}$ macro-CTA (3.26 g), and azobisisobutyronitrile (AIBN) (9.9 mg; macro-CTA/AIBN molar ratio = 5.0) were dissolved in a 85:15 w/w ethanol/water mixture. This reaction mixture was sealed in a round-bottomed flask, purged with nitrogen gas for 20 min, and then placed in a preheated oil bath at 70 °C for 8 h. The final BzMA conversion was determined using ^{1}H NMR analysis in CDCl$_3$ by comparing the integral of the two benzylic protons at 4.9 ppm assigned to PBzMA to that of the two vinyl protons corresponding to the BzMA monomer at 5.2 and 5.4 ppm.

Purification of Silica Particles. Commercial silica particles (AngstromSphere microspheres; nominal 500 nm diameter) were purified to remove any surface contamination via ultrasonication of a silica dispersion in isopropanol for 30 min, followed by centrifugation at 20 000 rpm for 30 min.[59] The alcoholic supernatant was carefully decanted and discarded. This clean-up protocol was repeated twice, and the purified silica particles were dried under vacuum at 30 °C overnight.

Heteroflocculation Protocol. Silica particles were dispersed in deionized water (pH 6.5) at 5.0 % w/w by stirring at 20 °C for 24 h.

PDMA$_{71}$−PBzMA$_{100}$ diblock copolymer nanoparticles dispersed in water (pH ≈ 6.5) at 1.0 % w/w were added to this aqueous silica dispersion, with nanoparticle adsorption occurring at 20 °C during roller mill mixing for 24 h. The number of nanoparticles per silica particle, N, was systematically varied to identify the critical value corresponding to the saturation coverage.

^{1}H NMR Spectroscopy. Monomer conversions for the synthesis of PDMA$_{71}$ macro-CTA and PDMA$_{71}$−PBzMA$_{100}$ diblock copolymers were determined using a Bruker AV1-400 MHz NMR spectrometer (64 scans recorded per spectrum in either CDCl$_3$ or CD$_2$Cl$_2$).

Gel Permeation Chromatography (GPC). The molecular weight distribution of the PDMA$_{71}$−PBzMA$_{100}$ diblock copolymer was assessed using GPC. The GPC set-up comprised two 5 μm (30 cm) "Mixed" columns and a WellChrom K-2301 refractive index detector operating at 950 ± 30 nm. THF eluent containing 2.0 w/w % triethylamine and 0.05 w/v % butylhydroxytoluene (BHT) was used at a flow rate of 1.0 mL min^{-1}. A series of ten near-monodisperse linear poly(methyl methacrylate) standards (M_p values ranging from 1280 to 330 000 g mol^{-1}) were purchased from Polymer Laboratories (Church Stretton, UK) and used for calibration, with the above refractive index detector.

Ultraviolet (UV) Absorption Spectroscopy. Copolymer adsorption onto silica particles was verified using UV spectroscopy. Aqueous dispersions of nanoparticle-coated silica particles were centrifuged at 5000 rpm for 25 min; then, the supernatant was carefully decanted in each case. An accurate volume of supernatant solution (2.00 mL) was dried under vacuum, and then the solid residues were dissolved in 1,4-dioxane. Absorption spectra were recorded using a dark-sided quartz cuvette of 1.0 cm path length and a Varian Cary 50 UV−visible spectrophotometer operating at a scan speed of 600 nm min^{-1}. For the Beer−Lambert calibration plot, aqueous PDMA$_{71}$−PBzMA$_{100}$ dispersions were dried at 30 °C using a vacuum oven and then dissolved in 1,4-dioxane to produce known copolymer concentrations. These solutions were serially diluted, and each absorbance was monitored at a λ_{max} of 307 nm. The molar absorption coefficient (ε) was determined from the linear absorbance versus concentration plot ($R^2 > 0.99$).

Diluted supernatants were analyzed for their absorption at $\lambda_{max} = 307$ nm, and the corresponding concentration of non-adsorbed PDMA$_{71}$−PBzMA$_{100}$ copolymer nanoparticles was calculated. Hence, the adsorbed amount in each case was determined by the difference.

Helium Pycnometry. The solid-state density of the purified silica particles was determined using a Micromeritics AccuPyc 1330 helium pycnometer operating at 20 °C.

Transmission Electron Microscopy (TEM). Copper/palladium TEM grids (Agar Scientific, UK) were surface-coated in-house with a thin film of amorphous carbon. The grids were subjected to a glow discharge for 30 s to create a hydrophilic surface. Each aqueous copolymer-coated silica dispersion (10 μL) was adsorbed onto a treated grid for 60 s and then blotted with filter paper to remove excess liquid. Uranyl formate (10 μL, 0.75 w/w % aqueous solution) was placed onto each loaded grid for 20 s and then blotted to remove excess liquid. The grids were dried using a vacuum hose. Imaging was performed using a Philips CM100 instrument operating at 100 kV and equipped with a Gatan 1k CCD camera.

X-ray Photoelectron Spectroscopy (XPS). Dispersions of copolymer-coated silica particles were centrifuged for 25 min at 5000 rpm. Each supernatant was carefully removed, and the sediment was dried under vacuum overnight. The dried copolymer-coated silica particles were pressed onto an indium foil before measurement. Control samples comprising bare silica particles and PDMA$_{71}$−PBzMA$_{100}$ copolymer nanoparticles were also prepared on the indium foil. XPS studies were conducted using a Kratos Axis Ultra "DLD" instrument equipped with a monochromatic Al Kα X-ray source ($h\nu$ = 1486.6 eV) operating at a base pressure in the range of 10^{-8} to 10^{-10} mbar.

Dynamic Light Scattering (DLS). Hydrodynamic particle diameters were determined using a Malvern Zetasizer NanoZS model ZEN 3600 instrument, equipped with a 4 mW He−Ne solid-state laser, operating at 633 nm. Back-scattered light was detected at

173°, and the mean particle diameter was calculated by the quadratic fitting of the correlation function using the Stokes−Einstein equation over thirty runs of 10 s duration. Highly dilute aqueous dispersions were analyzed using disposable plastic cuvettes at 25 °C; all measurements were performed three times, and mean particle diameters were reported.

Aqueous Electrophoresis. Zeta potentials and mobilities were determined for silica sols, copolymer nanoparticles, and various nanoparticle-coated silica particles dispersed in the presence of 1 mM KCl background salt using the same Malvern Zetasizer NanoZS instrument described above. The solution pH was adjusted manually using either 0.1 M KOH or 0.01 M HCl.

Small-Angle X-ray Scattering (SAXS). SAXS patterns were collected at a synchrotron source (Diamond Light Source, station I22, Didcot, UK) using monochromatic X-ray radiation (wavelength λ = 0.0998 nm, with q ranging from 0.01 to 0.2 Å^{-1}, where $q = 4\pi \sin \theta/\lambda$ is the length of the scattering vector and θ is half of the scattering angle) and a 2D Pilatus 2 M pixel detector (Dectris, Switzerland). Polycarbonate capillaries of 2.0 mm diameter were used as a sample holder. SAXS data were reduced (normalization and integration) using the Dawn software supplied by Diamond Light Source. Scattering data were further analyzed (background subtraction and data modeling) using Irena SAS macros for Igor Pro.[60] The structural model used for the SAXS data analysis is given in the Supporting Information. This model is based on the analytical expression for a spherical micelle form factor.[61]

Disk Centrifuge Photosedimentometry (DCP). A DC24000 instrument (CPS Instruments, USA) was used to obtain the weight-average particle size distributions. This disk centrifuge employs a 405 nm diode sensor for particle detection at the disk boundary. The rate of centrifugation used in the present study was 5124 rpm. After reaching this speed, a density gradient was generated in situ by filling the empty disk with an aqueous spin fluid (total volume = 14.4 mL). An 8−24 w/w % aqueous sucrose gradient was prepared by injecting 1.50 mL of nine aqueous sucrose solutions in turn (beginning with the most concentrated solution), followed by n-dodecane (0.50 mL) to extend the gradient lifetime. After equilibration for 20 min, the instrument was calibrated by injecting 100 µL of 476 nm near-monodisperse poly(vinyl chloride) latex particles (Analytik Ltd., UK) before each measurement. Particle size distributions for both bare silica and nanoparticle-coated silica particles were recorded after injection of a 0.25 w/w % aqueous dispersion in each case.

Thermogravimetric Analysis (TGA). Analyses were conducted using a Q500 TGA instrument (TA Instruments) on dried sediments of aqueous dispersions of nanoparticle-coated silica particles obtained after centrifugation for 25 min at 5000 rpm, followed by drying under vacuum. Each sample was heated under a nitrogen atmosphere and initially held at 100 °C for 30 min to ensure complete removal of water before heating up to 800 °C at 10 °C min^{-1}. The observed mass loss was attributed to the complete pyrolysis of the copolymer component, with the remaining incombustible residues attributed to silica. The bare silica particles also exhibited a mass loss of 4.5% owing to surface moisture. This value was used to correct the mass losses obtained for the nanoparticle-coated silica particles.

■ RESULTS AND DISCUSSION

PDMA macro-CTA was synthesized by RAFT solution polymerization in THF using a trithiocarbonate-based RAFT agent (PETTC; prepared as reported previously).[41] Following purification, ^{1}H NMR studies indicated a mean DP of 71 for this PDMA macro-CTA, which was then chain-extended with BzMA via RAFT dispersion polymerization in an 85:15 ethanol/water mixture (see Scheme 1a). ^{1}H NMR confirmed that almost complete BzMA polymerization occurred after 8 h at 70 °C; THF GPC analysis showed an increase in the molecular weight relative to that of the PDMA macro-CTA, and the relatively low final copolymer polydispersity (M_w/M_n = 1.28) indicated a well-controlled polymerization (see Figure

Scheme 1. (a) Synthesis of PDMA$_{71}$ Macro-CTA and Subsequent Chain Extension by RAFT Alcoholic Dispersion Polymerization of BzMA at 70 °C To Produce Sterically Stabilized PDMA$_{71}$–PBzMA$_{100}$ Diblock Copolymer Nanoparticles via PISA (PETTC/ACVA Molar Ratio = 10; PDMA/AIBN Molar Ratio = 5). (b) Schematic Cartoon Showing the Adsorption of Small Cationic Diblock Copolymer Nanoparticles onto Large Anionic Silica Spheres
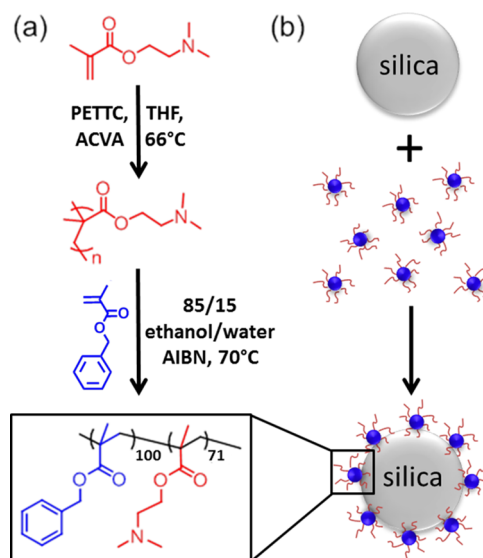
S1). PDMA−PBzMA diblock copolymer nanoparticles were synthesized at 15 w/w % solids and then diluted to 1.0 w/w % in water before mixing with silica particles, which serve as a model pigment.

An AngstromSphere silica sol was purified before use to remove any organic surface impurities.[59] Helium pycnometry indicated the density of the dried, purified silica sol to be 1.99 g cm^{-3}. This silica sol was then redispersed in deionized water at 5.0 w/w % solids before analysis. Figure 1a shows the TEM
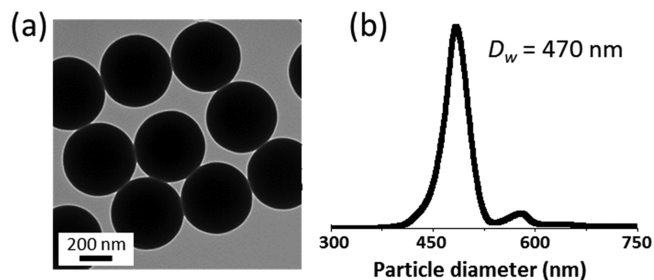

Figure 1. (a) TEM image of the AngstromSphere silica particles used in this work. (b) Particle size distribution obtained for this silica sol as determined using DCP using a silica density of 1.99 g cm^{-3}.

image of these purified silica particles. The particle size distribution was also assessed using DCP, which reported a D_w of 470 ± 17 nm for the major population, with an additional minor population at 580 nm corresponding to doublets (Figure 1b).

The PDMA$_{71}$−PBzMA$_{100}$ diblock copolymer nanoparticles were characterized using TEM, DLS, and SAXS (see Figure 2). DLS gave an intensity-average hydrodynamic diameter (D_H) of 30 ± 4 nm; TEM studies confirmed a spherical morphology with a number-average diameter (D_n) of 25 ± 3 nm (counting
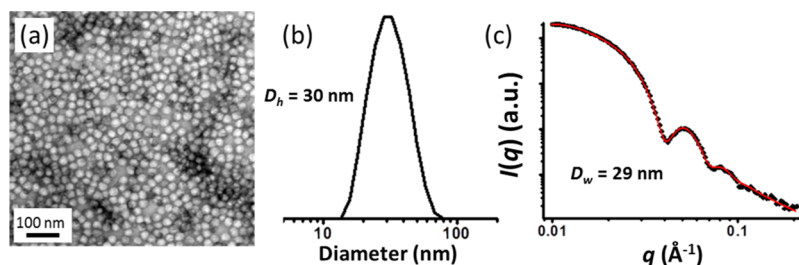
Figure 2. Particle size analysis of PDMA$_{71}$−PBzMA$_{100}$ diblock copolymer nanoparticles. (a) Representative TEM image showing a well-defined spherical morphology, (b) DLS particle size distribution, and (c) SAXS curve fitted using a spherical micelle model.
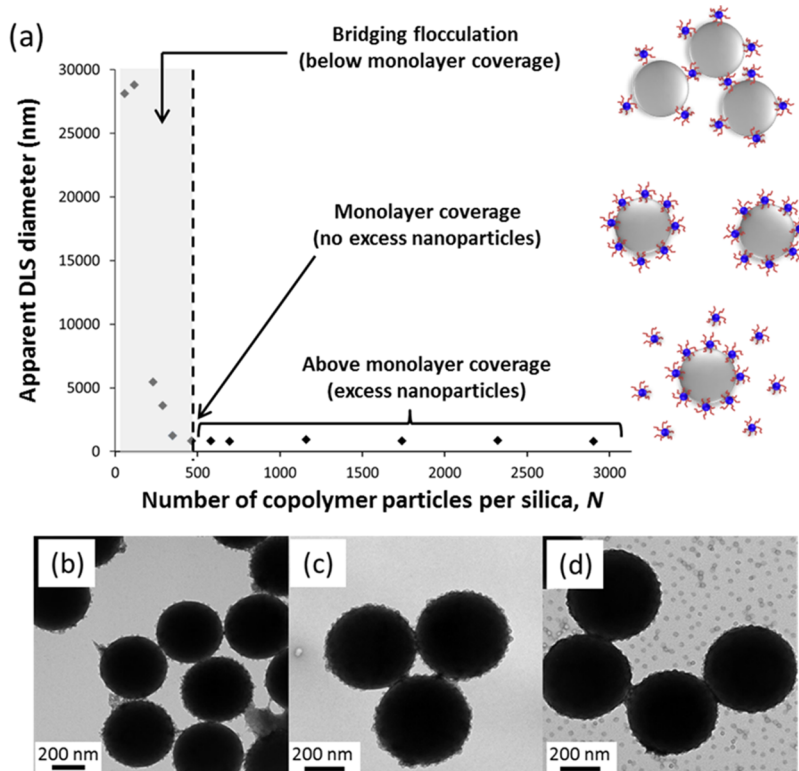

Figure 3. (a) Apparent DLS hydrodynamic diameter obtained for 470 nm-diameter anionic silica particles in the presence of differing amounts of cationic PDMA$_{71}$−PBzMA$_{100}$ copolymer nanoparticles. The vertical dashed line indicates the N value corresponding to the monolayer coverage. TEM images of (b) partially coated, flocculated silica particles, (c) well-coated silica particles with no nanoparticles present in the background, and (d) well-coated silica particles plus excess non-adsorbed copolymer nanoparticles.

more than 50 nanoparticles using ImageJ 1.48v software downloaded from http://imagej.nih.gov/ij/). PDMA$_{71}$−PBzMA$_{100}$ nanoparticle dispersions were diluted with water to 4.0 w/v % to minimize interparticle interactions in SAXS studies. The scattering curve expressed as a double logarithmic plot of $I(q)$ against q is shown in Figure 2c. This curve was fitted using a micelle model[61,62] assuming a Gaussian size distribution, yielding an overall weight-average diameter (D_w) of 29 ± 0.5 nm and a weight-average PBzMA-only core diameter of 19.6 ± 0.9 nm (see Supporting Information for further details). From this analysis, the radius of gyration of the PDMA stabilizer was calculated to be 2.4 nm and the mean aggregation number (N_{agg}) for the nanoparticles was determined to be 154 (with negligible solvation of the core-forming PBzMA block). The difference in size simply reflects the differing moments reported by each technique, as previously reported.[43] In addition, TEM is largely insensitive to the PDMA stabilizer layer, whereas SAXS and DLS account for this structural feature.

Aqueous dispersions of silica (5.0 w/w %) and PDMA$_{71}$−PBzMA$_{100}$ nanoparticles (1.0 w/w %) were mixed overnight to obtain nanoparticle-coated silica particles. The copolymer/silica mass ratio was systematically varied to identify the conditions corresponding to the monolayer coverage. The packing efficiency was calculated using the method reported by Balmer et al.[53] Hence the precise copolymer/silica mass ratio required for saturation coverage was determined. The number of silica spheres (n_s) and copolymer spheres (n_p) were calculated using eqs 1 and 2, respectively. Here, n_s and n_p depend on the mass of the components (m_s for the silica sol and m_p for copolymer nanoparticles), the mass density of silica (ρ_s), N_{agg} and the number-average molecular mass of the copolymer chains (M_n). The mean silica radius (r_s) is taken from the weight-average diameter reported using DCP. N is the mean number of added copolymer nanoparticles per silica particle, as shown in eq 3. The mean copolymer nanoparticle radius (r_p) is taken from the intensity-average diameter determined using DLS. The final packing efficiency (P) can then be calculated using the

geometric considerations for sphere-on-sphere packing (see eq 4).

$$n_s = \frac{m_s}{\rho_s (4/3 \pi r_s^3)} \qquad (1)$$

$$n_p = \frac{m_p}{N_{agg} M_n} \qquad (2)$$

$$N = \frac{n_p}{n_s} \qquad (3)$$

$$P = \frac{N r_s^2}{4(r_p + r_s)} \qquad (4)$$

N was systematically varied by fixing the silica concentration and varying the copolymer concentration to enable the construction of a plot of DLS hydrodynamic diameter against N (see Figure 3a). This plot was then used to estimate the critical value of N corresponding to the monolayer coverage, as described by Balmer et al.[53]

For N values greater than that of the inflection point (indicated by a vertical dashed line), the apparent particle diameters are relatively small and approximately constant, which indicates a high degree of dispersion owing to steric stabilization at or above saturation coverage of the silica particles by the cationic copolymer nanoparticles. In contrast, much larger apparent diameters were observed at lower N values, which correspond to lower coverage and hence bridging flocculation of the silica particles. This interpretation was supported by TEM observations: Figure 3b−d shows images recorded at selected N values. When $N < 465$ (i.e., below monolayer coverage), partially coated flocculated silica particles are observed (Figure 3b). At $N = 465$, the silica particles are well-coated with cationic nanoparticles (Figure 3c). Higher N values lead to excess copolymer nanoparticles being observed in the background, in addition to nanoparticle-coated silica particles (Figure 3d). For this system, saturation coverage was obtained at $N \approx 465$, which equates to $P = 0.42$ (or 42%). This fractional surface coverage is somewhat lower than that observed by Balmer et al., who reported $P = 0.69$ (or 69%) for 463 nm-diameter P2VP latex particles coated with 20 nm-diameter silica particles.[53] The lower surface coverages observed in the present study reflect both the sterically stabilized nature of the cationic nanoparticles and their strong electrostatic interactions with the anionic silica particles, which reduces the possibility of nanoparticle rearrangement after adsorption.

Aqueous electrophoresis was used to assess the electrostatic adsorption of the $PDMA_{71}-PBzMA_{100}$ diblock copolymer nanoparticles onto the silica particles. The silica particles are anionic at high pH as a result of ionization of their surface silanol groups. On the other hand, the diblock copolymer nanoparticles are cationic over a wide pH range because the PDMA stabilizer chains are protonated below their pK_a of approximately 7.5.[63] Thus adsorption of these cationic nanoparticles onto the anionic silica particles at around pH 7 leads to surface charge reversal and therefore a change in the overall zeta potential from negative to positive.

Electrophoretic mobilities (μ) were determined using phase analysis light scattering. As the nanoparticle radius is relatively small compared to the Debye length (κ^{-1}), the Helmholtz−Smoluchowski equation is not applicable.[64] However, as the

magnitude of the zeta potential is relatively low (< 50 mV),[64] the Henry equation can be used instead.[65] This equation includes a prefactor $f(\kappa a)$ term that has been calculated using Ohshima's equation for any value of κa, where κ is the inverse Debye length and a is the particle radius.[66]

Figure 4 shows the zeta potential versus pH curves obtained for $PDMA_{71}-PBzMA_{100}$ nanoparticles, bare silica particles, and
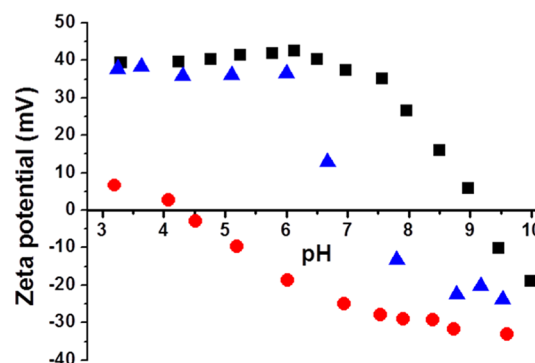

Figure 4. Aqueous electrophoresis data obtained for $PDMA_{71}-PBzMA_{100}$ diblock copolymer nanoparticles (black squares), bare 470 nm silica sol (red circles), and nanoparticle-coated silica particles (blue triangles).

the resultant nanoparticle-coated silica particles at saturation coverage ($N = 465$). The diblock copolymer nanoparticles are cationic at or below pH 9, the bare silica sol is anionic above pH 4, and the nanoparticle-coated silica particles exhibit an intermediate isoelectric point at around pH 7. Thus these data suggest that the cationic nanoparticles indeed adsorb onto the anionic silica particles. ($PDMA_{71}-PBzMA_{100}$ nanoparticles become anionic above pH 9 as a result of ionization of the terminal carboxylic acid groups derived from the RAFT CTA. Similar observations have been reported previously for this system[40,41]).

UV spectroscopy was used to assess the efficiency of copolymer nanoparticle adsorption. Figure 5a shows the absorption spectra recorded at 307 nm for copolymer solutions of known concentration in 1,4-dioxane. This is a good solvent for both blocks, which leads to nanoparticle dissolution and hence eliminates the problem of particle scattering at shorter wavelengths. The corresponding calibration plot (see Figure 5b) yielded the molar absorption coefficient for the trithiocarbonate end-group at this wavelength, which was used to determine the concentration of non-adsorbed nano-particles present in the supernatant. After mixing, the dispersions were centrifuged at 5000 rpm for 25 min, and the supernatant was carefully decanted. This was then dried, and the non-adsorbed copolymer was dissolved in 1,4-dioxane for analysis using UV spectroscopy. Figure 5c shows the amount of excess copolymer present for various N values. At $N \leq 465$, there is almost no residual copolymer, indicating that all nanoparticles have adsorbed onto the silica particles. Above this critical value, the amount of copolymer present in the supernatant increases as more copolymer is added, as expected.

To assess the mass of the adsorbed nanoparticles directly, TGA studies were conducted on the sedimented nanoparticle-coated silica particles obtained after centrifugation. Samples were heated at 100 °C for 30 min to correct for any mass loss due to the remaining solvent before heating up to 800 °C. The observed mass loss between 100 and 800 °C is attributed to the
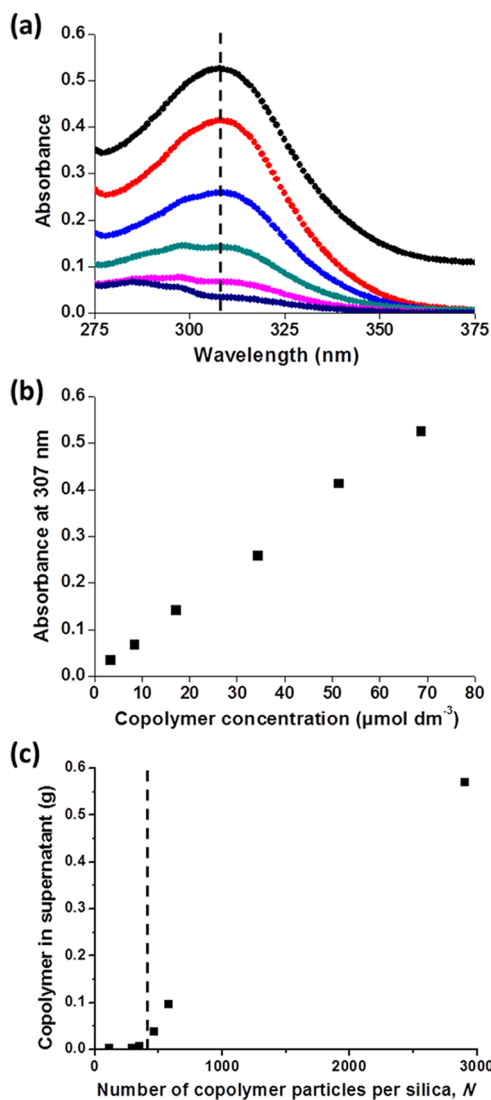
<>

Figure 5. (a) UV spectra recorded for known concentrations of PDMA$_{71}$−PBzMA$_{100}$ dissolved in 1,4-dioxane and (b) the corresponding calibration plot using the maximum absorbance at 307 nm to calculate the molar absorption coefficient (ε_{max} = 7600 ± 200 mol^{-1} dm^3 cm^{-1}). (c) Mass of PDMA$_{71}$−PBzMA$_{100}$ remaining in the supernatant after centrifugation of dispersions of nanoparticle-coated silica particles prepared at different mass ratios (the vertical dashed line corresponds to N = 465, or the saturation coverage).

pyrolysis of the adsorbed copolymer nanoparticles. Below saturation coverage, the nanoparticle-coated silica particles exhibited a monotonic increase in mass loss up to N = 465, for which the mass loss was approximately 3.3%. This is consistent with the UV spectroscopy analysis, which indicated that essentially all copolymer nanoparticles were adsorbed onto the silica particles up to N = 465. It was anticipated that all samples prepared at or above monolayer coverage would exhibit the same mass loss because all excess copolymer nanoparticles remaining in the supernatant should be removed before TGA. However, in practice, the experimental mass loss varied by ±0.5%, which is an indication of the experimental error associated with this protocol.

Nanoparticle-coated silica particles prepared at three different copolymer/silica mass ratios were analyzed using XPS. Theoretical surface coverages of the silica by the nanoparticles

were 31, 42, and 52%, respectively, as calculated using eq 4. A summary of the XPS data is given in Table 1.

Table 1. Theoretical Fractional Surface Coverage of the Silica Particles by PDMA$_{71}$−PBzMA$_{100}$ Copolymer Nanoparticles Calculated Using eq 4 Compared with Experimental XPS Data Calculated from the Normalized N1s Signal for the Copolymer Nanoparticles

sample ID	surface nitrogen content (atom %)	fractional surface coverage of silica particles	
		experimental	theoretical
below saturation coverage (N = 348)	2.0	0.40	0.31
saturation coverage (N = 465)	2.5	0.51	0.42
above saturation coverage (N = 581)	2.8	0.58	0.52
PDMA$_{71}$−PBzMA$_{100}$ nanoparticles	4.9	N/A	N/A
bare silica particles	0.0	N/A	N/A

X-ray photoelectron survey spectra confirmed the presence of the N1s signal (which serves as a unique elemental marker for the PDMA$_{71}$−PBzMA$_{100}$ copolymer nanoparticles) and the Si2p signal (which serves as a unique elemental marker for the silica component[67]). In all cases, underlying silica particles are detected in addition to the adsorbed layer of copolymer nanoparticles. Because the mean nanoparticle diameter exceeds the typical XPS sampling depth of 2−5 nm,[68] this indicates gaps between the adsorbed copolymer nanoparticles. This was expected given the relatively low theoretical fractional surface coverages calculated using eq 4 and reported in Table 1. Experimental values are calculated by comparing the surface nitrogen content of a given sample with that obtained for the pristine copolymer nanoparticles. The data in Table 1 indicate that the experimental fractional surface coverages determined using XPS follow the same trend as the theoretical values calculated using eq 4. However, the former values are somewhat higher in all cases, which may indicate perturbation of the original copolymer morphology after nanoparticle adsorption onto the silica particles. The experimental fractional surface coverage of 0.51 (or 51%) is comparable to that determined by Balmer et al. for the physical adsorption of silica nanoparticles on P2VP latexes.[53]

Aqueous electrophoresis measurements were performed for both bare and nanoparticle-coated silica particles (at pH 6.4). Electrophoretic mobilities (μ) were converted into zeta potentials using the Henry equation, as described earlier. The bare silica particles were highly anionic, as expected. On addition of cationic copolymer nanoparticles, this negative surface charge was first neutralized and then reversed (see Figure 6). Zeta potentials recorded for the nanoparticle-coated silica particles increased approximately linearly up to N = 290, and as N was further increased, the zeta potential reached a plateau value of around +40 mV. If the variation in the zeta potential at low N is subject to linear interpolation, then neutralization of the particle surface charge occurs at $N \approx 144$. According to Figure 3a, this critical value lies well within the bridging flocculation regime. The zeta potential continues to increase monotonically as more cationic nanoparticles are adsorbed, and the "knee" of this plot corresponds to approximately N = 465, or monolayer coverage.
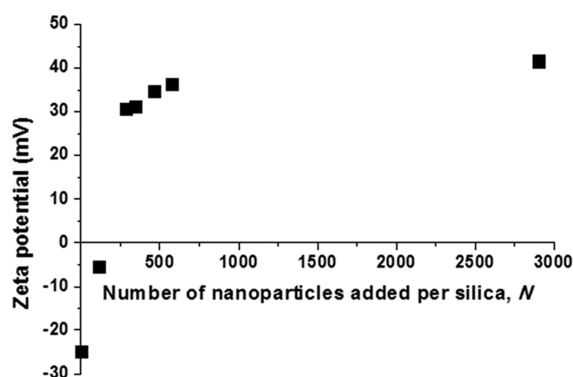
Figure 6. Change in the zeta potential recorded at pH 6.4 for nanoparticle-coated silica particles as a function of the number of copolymer nanoparticles added per silica particle, N. The zeta potential becomes approximately zero when $N = 144$ and reaches a plateau value of +40 mV for higher N values.

Adsorption of low-density copolymer nanoparticles onto silica leads to a lower effective density for the resulting nanoparticle-coated silica particles compared with that of bare silica particles. This is potentially of interest when formulating paints and coatings because such composite particles should be more buoyant within the aqueous phase and hence be less susceptible to gravitational settling over extended time periods. As stated earlier, DCP studies reported a mean weight-average diameter of 470 ± 17 nm for the bare silica sol (Figure 1b). However, using the solid-state silica density determined using helium pycnometry (1.99 g cm^{-3}) for the nanoparticle-coated silica particles leads to an erroneous underestimated weight-average diameter of 437 ± 20 nm. This artifact highlights the importance of correcting for the effective particle density in such centrifugal sizing measurements.

Figure 7 shows two possible scenarios for the PDMA$_{71}$–PBzMA$_{100}$ nanoparticles after their electrostatic adsorption onto the 470 nm silica particles: (1) no deformation of the PBzMA cores and (2) partial deformation of the PBzMA cores to form hemispheres (and hence a somewhat thinner adsorbed layer). The effective density of the nanoparticle-coated silica particles can be calculated theoretically from the sum of the volume fraction (φ)-weighted mass densities (ρ) using eq 5. Here the core is silica and the shell is a mixture of copolymer nanoparticles and the entrained solvent. To a good first approximation, the density of this shell can be taken to be 1.00

g cm^{-3} because of the relatively high volume fraction occupied by the solvent (water).

$$\rho_{particle} = \varphi_{core}\rho_{core} + \varphi_{shell}\rho_{shell} \qquad (5)$$

If no deformation of the PBzMA cores is assumed, then an upper limit of the shell thickness can be calculated. Based on SAXS measurements, the overall volume-average diameter of the sterically stabilized nanoparticles in solution is 29 nm. The R_g of the PDMA stabilizer chains is approximately 2.4 nm, suggesting a mean stabilizer layer thickness of 4.8 nm. Assuming that the stabilizer chains in direct contact with the silica surface are fully collapsed after nanoparticle adsorption, the shell thickness is calculated to be 24.2 nm. This gives a theoretical effective particle density of 1.74 g cm^{-3}. Alternatively, the PBzMA cores may become partially deformed after their adsorption onto the silica particles. In this case, the shell thickness can be estimated by assuming that the PBzMA cores form hemispheres on the silica surface, giving a mean adsorbed layer thickness of 14.5 nm and a corresponding theoretical effective particle density of 1.83 g cm^{-3}.

DCP was used to assess which of the two nanoparticle adsorption scenarios depicted in Figure 7 is likely to be physically realistic. Inputting a theoretical effective density of 1.74 g cm^{-3} produced a weight-average particle diameter of 524.9 nm (see Figure 8). This value lies quite close to the mean diameter of 470 nm + (2 × 24.2 nm) = 518.4 nm, calculated for the nanoparticle-coated silica particles; this corresponds to scenario 1 (i.e., retention of the original spherical nanoparticle morphology after adsorption). However, inputting the theoretical effective density of 1.83 g cm^{-3} suggested by scenario 2 produced a weight-average particle diameter of only 482.8 nm. This value lies further from the overall weight-average diameter of 470 nm + (2 × 14.5 nm) = 499 nm calculated for this alternative scenario, which assumes partially deformed adsorbed nanoparticles. In summary, the combined DCP and SAXS data suggest that the PBzMA cores remain essentially unperturbed after nanoparticle adsorption onto the silica particles, as represented by scenario 1 in Figure 7. The modest discrepancy between the theoretical and DCP-derived weight-average diameters is at least partly the result of assuming that the adsorbed PDMA chains in direct contact with the silica surface occupy negligible volume. We note that the lack of deformation of the nanoparticle cores during adsorption is consistent with the minimal solvation of the PBzMA chains indicated by SAXS analysis. Moreover, TEM studies of
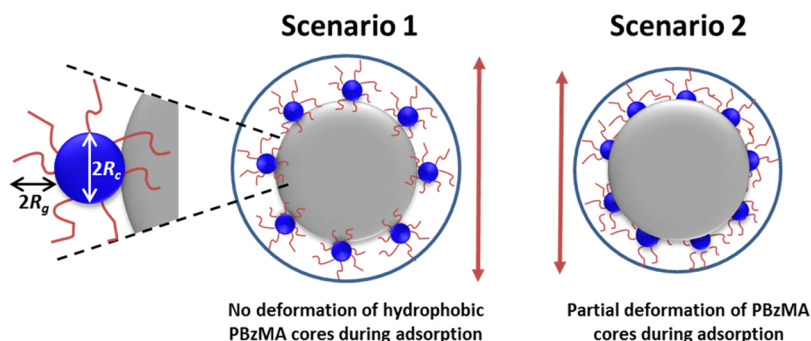

Figure 7. Schematic cartoon showing PDMA$_{71}$–PBzMA$_{100}$ diblock copolymer nanoparticles adsorbed onto 470 nm silica particles for two differing adsorption scenarios. Scenario 1 corresponds to no deformation of hydrophobic PBzMA cores during adsorption, whereas scenario 2 depicts a partial deformation of these PBzMA cores during adsorption to form hemispheres (and hence a somewhat thinner adsorbed layer of nanoparticles). In both cases, the red cationic stabilizer chains in direct contact with the anionic silica surface are collapsed and occupy negligible volume.
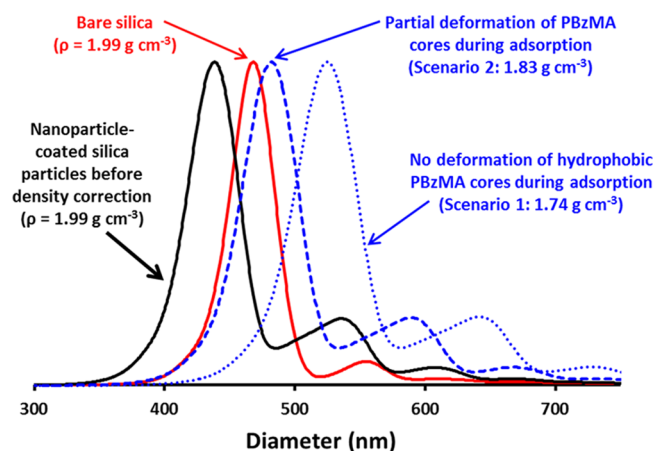
Figure 8. Normalized weight-average particle size distributions obtained using DCP for bare silica particles (density = 1.99 g cm^{-3}) and nanoparticle-coated silica particles before and after correction for their effective particle densities. The combined DCP and SAXS data suggest that the PBzMA cores remain essentially unperturbed after nanoparticle adsorption onto the silica particles (see schematic cartoon depicting scenario 1 in Figure 7).

somewhat larger PDMA$_{71}$−PBzMA$_{500}$ nanoparticles adsorbed onto 470 nm silica particles provide direct experimental evidence for retention of the original spherical nanoparticle morphology (see Figure S2).

CONCLUSIONS

In summary, we have examined the electrostatic adsorption of small sterically stabilized cationic diblock copolymer nanoparticles onto large anionic silica particles, which serve as a model pigment for aqueous formulations. This study demonstrates that copolymers can act as effective dispersants when present in nanoparticle form, rather than as molecularly dissolved chains. Relatively high degrees of dispersion can be achieved either at or above saturation coverage of the silica particles, whereas extensive bridging flocculation is observed at lower coverages. The combination of SAXS and disk centrifuge data suggests that the copolymer nanoparticles adsorb onto silica without significant perturbation of their original morphology. Such systems enhance our understanding of the problem of effective particle density and are also likely to be of interest for certain advanced aqueous pigment and coating formulations.

ASSOCIATED CONTENT

Ⓢ Supporting Information

The Supporting Information is available free of charge on the ACS Publications website at DOI: 10.1021/acs.langmuir.6b04541.

> GPC curves, TEM image showing PDMA$_{71}$−PBzMA$_{500}$ diblock copolymer nanoparticles adsorbed onto 470 nm silica particles, and full details of the spherical micelle model used for SAXS analysis (PDF)

AUTHOR INFORMATION

Corresponding Authors
*E-mail: lizzy.jones@sheffield.ac.uk (E.R.J.).
*E-mail: s.p.armes@shef.ac.uk (S.P.A.).

ORCID Ⓞ
S. P. Armes: 0000-0002-8289-6351

Notes
The authors declare no competing financial interest.

REFERENCES

(1) Burnett, G. M.; Paton, C.; Meares, P. Styrene + methyl methacrylate block copolymers. Part 2—Behaviour in dilute solutions. *Trans. Faraday Soc.* **1962**, *58*, 737−746.

(2) Krause, S. Dilute solution properties of a styrene—methyl methacrylate block copolymer. *J. Phys. Chem.* **1964**, *68*, 1948−1955.

(3) Lewis, P. R.; Price, C. Morphology of ABA block polymers. *Nature* **1969**, *223*, 494−495.

(4) Zhang, L.; Eisenberg, A. Multiple morphologies of "crew-cut" aggregates of polystyrene-*b*-poly(acrylic acid) block copolymers. *Science* **1995**, *268*, 1728−1731.

(5) Wilhelm, M.; Zhao, C. L.; Wang, Y.; Xu, R.; Winnik, M. A.; Mura, J. L.; Riess, G.; Croucher, M. D. Poly(styrene−ethylene oxide) block copolymer micelle formation in water: A fluorescence probe study. *Macromolecules* **1991**, *24*, 1033−1040.

(6) Xu, R.; Winnik, M. A.; Hallett, F. R.; Riess, G.; Croucher, M. D. Light-scattering study of the association behavior of styrene−ethylene oxide block copolymers in aqueous solution. *Macromolecules* **1991**, *24*, 87−93.

(7) Gao, Z.; Eisenberg, A. A model of micellization for block copolymers in solutions. *Macromolecules* **1993**, *26*, 7353−7360.

(8) Qin, A.; Tian, M.; Ramireddy, C.; Webber, S. E.; Munk, P.; Tuzar, Z. Polystyrene−poly(methacrylic acid) block copolymer micelles. *Macromolecules* **1994**, *27*, 120−126.

(9) Baines, F. L.; Armes, S. P.; Billingham, N. C.; Tuzar, Z. Micellization of poly(2-(dimethylamino)ethyl methacrylate-*block*-methyl methacrylate) copolymers in aqueous solution. *Macromolecules* **1996**, *29*, 8151−8159.

(10) Förster, S.; Zisenis, M.; Wenz, E.; Antonietti, M. Micellization of strongly segregated block copolymers. *J. Chem. Phys.* **1996**, *104*, 9956−9970.

(11) Moffitt, M.; Khougaz, K.; Eisenberg, A. Micellization of ionic block copolymers. *Acc. Chem. Res.* **1996**, *29*, 95−102.

(12) Li, H.; Yu, G.-E.; Price, C.; Booth, C.; Hecht, E.; Hoffmann, H. Concentrated aqueous micellar solutions of diblock copoly-(oxyethylene/oxybutylene) E$_{41}$B$_8$: A study of phase behavior. *Macromolecules* **1997**, *30*, 1347−1354.

(13) Won, Y.-Y.; Davis, H. T.; Bates, F. S. Giant Wormlike Rubber Micelles. *Science* **1999**, *283*, 960−963.

(14) Discher, B. M.; Won, Y.-Y.; Ege, D. S.; Lee, J. C.-M.; Bates, F. S.; Discher, D. E.; Hammer, D. A. Polymersomes: Tough Vesicles Made from Diblock Copolymers. *Science* **1999**, *284*, 1143−1146.

(15) Booth, C.; Attwood, D. Effects of block architecture and composition on the association properties of poly(oxyalkylene) copolymers in aqueous solution. *Macromol. Rapid Commun.* **2000**, *21*, 501−527.

(16) Discher, D. E.; Eisenberg, A. Polymer Vesicles. *Science* **2002**, *297*, 967−973.

(17) Antonietti, M.; Förster, S. Vesicles and liposomes: A self-assembly principle beyond lipids. *Adv. Mater.* **2003**, *15*, 1323−1333.

(18) Rodríguez-Hernández, J.; Chécot, F.; Gnanou, Y.; Lecommandoux, S. Toward "smart" nano-objects by self-assembly of block copolymers in solution. *Prog. Polym. Sci.* **2005**, *30*, 691−724.

(19) Bang, J.; Jain, S.; Li, Z.; Lodge, T. P.; Pedersen, J. S.; Kesselman, E.; Talmon, Y. Sphere, cylinder, and vesicle nanoaggregates in poly(styrene-*b*-isoprene) diblock copolymer solutions. *Macromolecules* **2006**, *39*, 1199−1208.

(20) Charleux, B.; Delaittre, G.; Rieger, J.; D'Agosto, F. Polymerization-Induced Self-Assembly: From Soluble Macromolecules to Block Copolymer Nano-Objects in One Step. *Macromolecules* **2012**, *45*, 6753−6765.

(21) Jakubauskas, H. L. Use of A−B block polymers as dispersants for nonaqueous coating systems. *J. Coat. Technol.* **1986**, *58*, 71−82.

(22) Spinelli, H. J. Group transfer polymerization and its use in water based pigment dispersants and emulsion stabilizers. *Prog. Org. Coat.* **1996**, *27*, 255−260.

(23) Creutz, S.; Jérôme, R.; Kaptijn, G. M. P.; van der Werf, A. W.; Akkerman, J. M. Design of polymeric dispersants for waterborne coatings. *J. Coat. Technol.* **1998**, *70*, 41−46.

(24) Duivenvoorde, F. L.; van Nostrum, C. F.; van der Linde, R. The pigmentation of powder coatings with the use of block copolymer dispersants. *Prog. Org. Coat.* **1999**, *36*, 225−230.

(25) Duivenvoorde, F. L.; van Nostrum, C. F.; Laven, J.; van der Linde, R. Improving pigment dispersing in powder coatings with block copolymer dispersants. *J. Coat. Technol.* **2000**, *72*, 145−152.

(26) Creutz, S.; Jérôme, R. Effectiveness of block copolymers as stabilizers for aqueous titanium dioxide dispersions of a high solid content. *Prog. Org. Coat.* **2000**, *40*, 21−29.

(27) Auschra, C.; Eckstein, E.; Mühlebach, A.; Zink, M.-O.; Rime, F. Design of new pigment dispersants by controlled radical polymerization. *Prog. Org. Coat.* **2002**, *45*, 83−93.

(28) D'Oliveira, J. M. R.; Xu, R.; Jensma, T.; Winnik, M. A.; Hruska, Z.; Hurtrez, G.; Riess, G.; Martinho, J. M. G.; Croucher, M. D. Direct adsorption of polystyrene−poly(ethylene oxide) micelles in water onto polystyrene latex particles. *Langmuir* **1993**, *9*, 1092−1097.

(29) Lin, Y.; Alexandridis, P. Temperature-dependent adsorption of Pluronic F127 block copolymers onto carbon black particles dispersed in aqueous media. *J. Phys. Chem. B* **2002**, *106*, 10834−10844.

(30) Sarkar, B.; Venugopal, V.; Tsianou, M.; Alexandridis, P. Adsorption of Pluronic block copolymers on silica nanoparticles. *Colloids Surf., A* **2013**, *422*, 155−164.

(31) Growney, D. J.; Mykhaylyk, O. O.; Armes, S. P. Micellization and Adsorption Behavior of a Near-Monodisperse Polystyrene-Based Diblock Copolymer in Nonpolar Media. *Langmuir* **2014**, *30*, 6047−6056.

(32) Growney, D. J.; Mykhaylyk, O. O.; Middlemiss, L.; Fielding, L. A.; Derry, M. J.; Aragrag, N.; Lamb, G. D.; Armes, S. P. Is Carbon Black a Suitable Model Colloidal Substrate for Diesel Soot? *Langmuir* **2015**, *31*, 10358−10369.

(33) Charleux, B.; D'Agosto, F.; Delaittre, G. Preparation of Hybrid Latex Particles and Core−Shell Particles through the Use of Controlled Radical Polymerization Techniques in Aqueous Media. *Adv. Polym. Sci.* **2010**, *233*, 125−183.

(34) Wan, W.-M.; Pan, C.-Y. One-pot synthesis of polymeric nanomaterials via RAFT dispersion polymerization induced self-assembly and re-organization. *Polym. Chem.* **2010**, *1*, 1475−1484.

(35) Monteiro, M. J.; Cunningham, M. F. Polymer Nanoparticles via Living Radical Polymerization in Aqueous Dispersions: Design and Applications. *Macromolecules* **2012**, *45*, 4939−4957.

(36) Warren, N. J.; Armes, S. P. Polymerization-Induced Self-Assembly of Block Copolymer Nano-Objects via RAFT Aqueous Dispersion Polymerization. *J. Am. Chem. Soc.* **2014**, *136*, 10174−10185.

(37) Derry, M. J.; Fielding, L. A.; Armes, S. P. Polymerization-induced self-assembly of block copolymer nanoparticles via RAFT non-aqueous dispersion polymerization. *Prog. Polym. Sci.* **2016**, *52*, 1−18.

(38) Canning, S. L.; Smith, G. N.; Armes, S. P. A Critical Appraisal of RAFT-Mediated Polymerization-Induced Self-Assembly. *Macromolecules* **2016**, *49*, 1985−2001.

(39) Zhang, X.; Rieger, J.; Charleux, B. Effect of the solvent composition on the morphology of nano-objects synthesized via RAFT polymerization of benzyl methacrylate in dispersed systems. *Polym. Chem.* **2012**, *3*, 1502−1509.

(40) Semsarilar, M.; Jones, E. R.; Blanazs, A.; Armes, S. P. Efficient Synthesis of Sterically-Stabilized Nano-Objects via RAFT Dispersion Polymerization of Benzyl Methacrylate in Alcoholic Media. *Adv. Mater.* **2012**, *24*, 3378−3382.

(41) Jones, E. R.; Semsarilar, M.; Blanazs, A.; Armes, S. P. Efficient Synthesis of Amine-Functional Diblock Copolymer Nanoparticles via RAFT Dispersion Polymerization of Benzyl Methacrylate in Alcoholic Media. *Macromolecules* **2012**, *45*, 5091−5098.

(42) Jones, E. R.; Semsarilar, M.; Wyman, P.; Boerakker, M.; Armes, S. P. Addition of water to an alcoholic RAFT PISA formulation leads to faster kinetics but limits the evolution of copolymer morphology. *Polym. Chem.* **2016**, *7*, 851−859.

(43) Jones, E. R.; Mykhaylyk, O. O.; Semsarilar, M.; Boerakker, M.; Wyman, P.; Armes, S. P. How Do Spherical Diblock Copolymer Nanoparticles Grow during RAFT Alcoholic Dispersion Polymerization? *Macromolecules* **2016**, *49*, 172−181.

(44) Kayes, J. B.; Rawlins, D. A. Adsorption characteristics of certain polyoxyethylene−polyoxypropylene block co-polymers on polystyrene latex. *Colloid Polym. Sci.* **1979**, *257*, 622−629.

(45) Stuart, M. A. C.; Cosgrove, T.; Vincent, B. Experimental aspects of polymer adsorption at solid/solution interfaces. *Adv. Colloid Interface Sci.* **1985**, *24*, 143−239.

(46) Luckham, P. F.; Vincent, B.; Tadros, T. F. The controlled flocculation of particulate dispersions using small particles of opposite charge. IV. Effect of surface coverage of adsorbed polymer on heteroflocculation. *Colloids Surf.* **1983**, *6*, 119−133.

(47) Skuse, D. R.; Tadros, T. F.; Vincent, B. Controlled heteroflocculation of non-aqueous silica dispersions. *Colloids Surf.* **1986**, *17*, 343−360.

(48) Islam, A. M.; Chowdhry, B. Z.; Snowden, M. J. Temperature-induced heteroflocculation in particulate colloidal dispersions. *J. Phys. Chem.* **1995**, *99*, 14205−14206.

(49) Balmer, J. A.; Mykhaylyk, O. O.; Fairclough, J. P. A.; Ryan, A. J.; Armes, S. P.; Murray, M. W.; Murray, K. A.; Williams, N. S. J. Unexpected Facile Redistribution of Adsorbed Silica Nanoparticles between Latexes. *J. Am. Chem. Soc.* **2010**, *132*, 2166−2168.

(50) Harley, S.; Thompson, D. W.; Vincent, B. The adsorption of small particles onto larger particles of opposite charge direct electron microscope studies. *Colloids Surf.* **1992**, *62*, 163−176.

(51) Ottewill, R. H.; Schofield, A. B.; Waters, J. A.; Williams, N. S. J. Preparation of core−shell polymer colloid particles by encapsulation. *Colloid Polym. Sci.* **1997**, *275*, 274−283.

(52) Au, K. M.; Armes, S. P. Heterocoagulation as a Facile Route to Prepare Stable Serum Albumin-Nanoparticle Conjugates for Biomedical Applications: Synthetic Protocols and Mechanistic Insights. *ACS Nano* **2012**, *6*, 8261−8279.

(53) Balmer, J. A.; Armes, S. P.; Fowler, P. W.; Tarnai, T.; Gáspár, Z.; Murray, K. A.; Williams, N. S. J. Packing Efficiency of Small Silica Particles on Large Latex Particles: A Facile Route to Colloidal Nanocomposites. *Langmuir* **2009**, *25*, 5339−5347.

(54) Balmer, J. A.; Le Cunff, E. C.; Armes, S. P.; Murray, M. W.; Murray, K. A.; Williams, N. S. J. When Does Silica Exchange Occur between Vinyl Polymer−Silica Nanocomposite Particles and Sterically Stabilized Latexes? *Langmuir* **2010**, *26*, 13662−13671.

(55) Balmer, J. A.; Mykhaylyk, O. O.; Armes, S. P.; Fairclough, J. P. A.; Ryan, A. J.; Gummel, J.; Murray, M. W.; Murray, K. A.; Williams, N. S. J. Time-Resolved Small-Angle X-ray Scattering Studies of Polymer−Silica Nanocomposite Particles: Initial Formation and Subsequent Silica Redistribution. *J. Am. Chem. Soc.* **2011**, *133*, 826−837.

(56) Bardman, J. K.; Brown, W. T.; Donnelly, K. M.; Zhang, W.; Lieser, B. H. Polymer−pigment composites. U.S. Patent 6576051 B2, 2003.

(57) van den Berg, A. M. J.; de Laat, A. W. M.; Smith, P. J.; Perelaer, J.; Schubert, U. S. Geometric control of inkjet printed features using a gelating polymer. *J. Mater. Chem.* **2007**, *17*, 677−683.

(58) Shin, H.-i.; Min, B. G.; Jeong, W.; Park, C. Amphiphilic block copolymer micelles: New dispersant for single wall carbon nanotubes. *Macromol. Rapid Commun.* **2005**, *26*, 1451−1457.

(59) Pilon, L. N. *Synthesis and Characterisation of Hydroxyl-Functional Polymers by ATRP*; University of Sussex, 2004.

(60) Ilavsky, J.; Jemian, P. R. Irena: Tool suite for modeling and analysis of small-angle scattering. *J. Appl. Crystallogr.* **2009**, *42*, 347−353.

(61) Pedersen, J. S.; Svaneborg, C.; Almdal, K.; Hamley, I. W.; Young, R. N. A small-angle neutron and X-ray contrast variation scattering study of the structure of block copolymer micelles: Corona shape and excluded volume interactions. *Macromolecules* **2003**, *36*, 416−433.

(62) Pedersen, J. S.; Gerstenberg, M. C. The structure of P85 Pluronic block copolymer micelles determined by small-angle neutron scattering. *Colloids Surf., A* **2003**, *213*, 175−187.

(63) Bütün, V.; Armes, S. P.; Billingham, N. C. Synthesis and aqueous solution properties of near-monodisperse tertiary amine methacrylate homopolymers and diblock copolymers. *Polymer* **2001**, *42*, 5993−6008.

(64) Delgado, A. V.; González-Caballero, F.; Hunter, R. J.; Koopal, L. K.; Lyklema, J. Measurement and Interpretation of Electrokinetic Phenomena (IUPAC Technical Report). *Pure Appl. Chem.* **2005**, *77*, 1753.

(65) Henry, D. C. The Cataphoresis of Suspended Particles. Part I. The Equation of Cataphoresis. *Proc. R. Soc. London, Ser. A* **1931**, *133*, 106−129.

(66) Ohshima, H. A Simple Expression for Henry's Function for the Retardation Effect in Electrophoresis of Spherical Colloidal Particles. *J. Colloid Interface Sci.* **1994**, *168*, 269−271.

(67) Maeda, S.; Gill, M.; Armes, S. P.; Fletcher, I. W. Surface characterization of conducting polymer−silica nanocomposites by X-ray photoelectron spectroscopy. *Langmuir* **1995**, *11*, 1899−1904.

(68) Watts, J. F.; Wolstenholme, J. *An Introduction to Surface Analysis by XPS and AES*; Wiley, 2003.